Fatigue of polycrystalline silicon for MEMS applications: crack growth and stability under resonant loading conditions

C. L. Muhlstein[a*], R.T. Howe[b], and R.O. Ritchie[a*]

[a]Materials Sciences Division, Lawrence Berkeley National Laboratory, and Department of Materials Science and Engineering, University of California, Berkeley, CA 94720
[b]Department of Electrical Engineering and Computer Science, University of California, Berkeley, CA 94720

Abstract

Although bulk silicon is not known to exhibit susceptibility to cyclic fatigue, micron-scale structures made from silicon films are known to be vulnerable to degradation by fatigue in ambient air environments, a phenomenon that has been recently modeled in terms of a mechanism of sequential oxidation and stress-corrosion cracking of the native oxide layer. To date, most stress-life (*S/N*) fatigue tests on such silicon films have been conducted using resonant-loaded specimens, where there has been a need to establish the interaction between the resonance and the driving force for fatigue-crack growth. In this paper, numerical analyses are used to establish the relationship between natural frequency, specimen compliance, and linear-elastic stress-intensity factor for a commonly used micron-scale, micromechanical fatigue characterization structure. Results are incorporated into a general, lumped, dynamic fatigue-crack stability model to evaluate the stability of fatigue cracks in resonant-loaded structures. As the applied stress amplitude and corresponding driving force for crack advance depend on the system damping as well as sample geometry in such resonant structures, changes in damping caused by cycling in different environments can have a significant mechanical effect on the stability of fatigue cracks. It is shown that testing *in vacuo*, which lowers the system damping, can lead to crack arrest, an effect which is independent of the absence of any environmental contribution to crack growth. Finally, the finite element models are applied to polycrystalline silicon structural films to determine the critical crack sizes (~5.5 to 66 nm) and an average fracture toughness (~0.85 MPa√m) from specimens subjected to fatigue cycling at stress amplitudes ranging from ~2.2 to 3.5 GPa.

Keywords: Fatigue, MEMS, Resonance, Polycrystalline Silicon, Crack Stability

1. Introduction

For the characterization of fatigue behavior with either total-life or fracture-mechanics methodologies, there is a need to simulate the cyclic stresses, fatigue lifetimes (i.e. cycles to failure), and crack-growth rates in the laboratory. This requires the application of cyclic forces to test specimens at reasonably high frequencies. In actuality, the loading frequency sets practical limits on the maximum fatigue lives and minimum crack-growth rates that can be measured. Where large numbers of cycles are required, electromechanical and resonant systems are often employed; indeed, with the developing emphasis on "gigacycle" fatigue (Stanzl-Tschegg and Mayer, 2001) and microelectromechanical systems (MEMS), there has

* Corresponding authors. Tel.: 001 510 486-4584, 5798; fax: 001 510 486-4995.
E-mail addresses: cmuhlstn@uclink4.berkeley.edu (C.L. Muhlstein); roritchie@lbl.gov (R.O. Ritchie)

been a renewed interest in such testing. Macroscale resonant fatigue testing systems often involve axial fatigue testing and fracture mechanics-style specimens, and have been used for both stress-life and crack-growth studies (e.g., ref. (Mayer, 1999)). In contrast, the micromechanical fatigue systems used for micron-scale fatigue testing generally behave like simple harmonic oscillators consisting of an elastic specimen (i.e., a spring) attached to a mass. Indeed, the micromechanical resonant fatigue characterization structure shown in Figure 1 has been widely used to evaluate the fatigue behavior of thin structural films of mono and polycrystalline silicon for MEMS applications (Allameh, et al., 2000; Brown, et al., 1997; Muhlstein, et al., 2000; Muhlstein, et al., 2001a; Muhlstein, et al., 2001b; Muhlstein, et al., 2001c; Muhlstein, et al., 2001d; Van Arsdell, 1997; Van Arsdell and Brown, 1999).

Despite its poor damage tolerance and low fracture toughness (~1 MPa√m (Ballarini, et al., 1997; Chen and Leipold, 1980; Kahn, et al., 1999b; St. John, 1975; Wong and Holbrook, 1987)), silicon has emerged as the dominant structural material for MEMS. Given the absence of plasticity and crack-tip shielding phenomena at room temperature, one would not anticipate thin-film silicon to be vulnerable to failure via traditional ductile or brittle material fatigue mechanisms (Ritchie, 1999; Suresh, 1998). However, using micromechanical resonant fatigue characterization structures similar to that shown in Figure 1, a number of investigations have demonstrated that micron-scale silicon exhibits "metal-like" stress-life (*S*/*N*) fatigue behavior in ambient air (Figure 10) (Brown, et al., 1997; Kahn, et al., 1999a; Kapels, et al., 1999; Muhlstein, et al., 2000; Muhlstein, et al., 2001a; Muhlstein, et al., 2001b). Our recent studies have indicated that the fatigue degradation process occurs via mechanisms confined to the SiO_2 native oxide layer that forms upon exposure to the atmosphere (Muhlstein, et al., 2001c; Muhlstein, et al., 2001d); specifically, this *reaction-layer fatigue* process involves the sequential, stress-assisted oxidation and stress-corrosion cracking of the native oxide, as described in ref. (Muhlstein, et al., 2001c). However, to fully understand how such fatigue damage accumulates in these *S*/*N* fatigue tests, it is necessary to fully characterize the micromechanical fatigue testing structure, and in particular to calculate the driving force for crack advance under resonant loading conditions.

During micromechanical fatigue characterization of silicon films, the compliance of the specimen increases as fatigue damage accumulates in the form of incipient crack growth. This degradation induces a corresponding decrease in the natural frequency of the structure. Much like macroscopic, fracture mechanics-based investigations (e.g. refs. (Chati, et al., 1997; Chondros, et al., 1998; Mahmoud, et al., 1999; McGuire, et al., 1995; Yokoyama and Chen, 1998), this change in specimen compliance can be correlated with crack growth through analytical or numerically-based models. What is less obvious is that this change in natural frequency can lead to a rapid reduction in the stress amplitude, as depicted schematically in Figure 2. Thus, the driving force for fatigue failure depends not only on the specimen geometry, but also on the damping in the system. Accordingly, the development of appropriate models of the fatigue characterization structure is a crucial step in understanding the fatigue damage accumulation in polycrystalline silicon.

The primary objectives of this work were to evaluate the fatigue-crack growth behavior and fracture toughness of polycrystalline silicon thin films and to determine the stability of the cracks under resonant loading conditions used in the fatigue characterization structure shown in Figure 1. First, finite element methods were used to evaluate the dynamic behavior and stress distribution of an uncracked structure. Similar models of a cracked structure were

then developed to determine the natural frequency and linear elastic crack-tip parameter, K. These models were then employed in a lumped, dynamic model of the micromechanical fatigue characterization structure to evaluate the stability of fatigue cracks. Finally, the finite element and lumped parameter numerical models of the structure were applied to experimental data from previous stress-life fatigue tests to evaluate the crack-growth rate and fracture toughness behavior of the *n*-type, thin film, polycrystalline silicon.

2. Experimental and Numerical Methods

To determine the natural frequency, compliance, and stress distribution for the fatigue characterization structure shown in Figure 1, dynamic and quasi-static finite element models were applied to both uncracked and cracked structures. In the case of the cracked structure the relationships between the crack length and the natural frequency and the stress intensity-factor, K, were also determined.

2.1. Micromechanical fatigue testing

The fatigue characterization structure (Fig. 1) used for thin-film silicon *S/N* fatigue testing was originally developed by Van Arsdell (Van Arsdell, 1997). This structure is ~300 μm square, and is analogous to a specimen, electromechanical load frame, and capacitive displacement transducer found in a conventional mechanical testing system. The specimen is a notched cantilever beam that is in turn attached to a large, perforated plate that serves as a resonant mass. The mass and beam are electrostatically forced to resonate and the resulting motion is measured capacitively. On opposite sides of the resonant mass are interdigitated "fingers" commonly referred to as "comb drives." One side of these drives is for electrostatic actuation; the other side provides capacitive sensing of motion. The resonance generates fully reversed, constant amplitude, sinusoidal stresses at the notch, i.e., a load ratio, R (ratio of minimum to maximum load), of -1. The structure is designed for testing at ~40 kHz and is excited at a fixed frequency that is updated periodically during the test. The notched beam specimens are ~40 μm long, 19.5 μm wide, and 2 μm thick. A 13 μm deep notch is located 9.8 μm from the base and has a root radius of about 1 μm based on scanning electron micrographs (SEM) of the structures. The toroidal plate spanning 60° (inner radius, r_{inner} = 30 μm, outer radius, r_{outer} = 300 μm, thickness, t = 1.97 μm) rotates about the midpoint of the remaining ligament of the notched beam and serves as a mass to lower the natural frequency of the structure. The specimens are tested at a constant applied electrostatic force amplitude until failure occurs by complete separation of the beam at the notch. During the test, the natural frequency of the structure decreases as fatigue damage accumulates at the notch. The natural frequency of the structure is periodically characterized (about every 60 seconds) throughout the fatigue test by measuring the amplitude of the resonance as the excitation frequency is varied by ±50 Hz around the resonant frequency of the structure, f. The dynamic response of the structure is fit with a second-order polynomial and the maximum is taken as an estimate of the resonant frequency. The fatigue characterization structure is then excited at this frequency with a constant force amplitude until the frequency sweep and curve fit are repeated (Muhlstein, et al., 2001a). The motion is measured via the rate of change of capacitance, calibrated using the method detailed in ref. (Muhlstein, et al., 2001a), and is monitored during every test. Thus, the natural frequency as a function of time data are a

record of damage accumulation; in addition, loss of resonance indicates specimen failure. The applied stress amplitude and crack-growth behavior are determined from the finite element methods described herein.

In total, 28 specimens of *n*-type polycrystalline silicon, ~2-μm thick films were tested to failure and the natural frequency as a function of time monitored. In previous studies, the fracture surfaces, crack paths, and microstructure were examined in detail (Muhlstein, et al., 2001a). In this study, the focus of the work is on the interpretation of the change in natural frequency and the stability of cracks in the specimen.

The design of the micromechanical fatigue characterization structure is amenable to a wide range of processing techniques and material systems, and has been used for studies of both silicon and silicon-germanium structural films. During a recent fabrication run of a polycrystalline SiGe surface micromachining process (Franke, et al., 2000), in addition to the "standard" notched cantilever beam geometry, a new specimen variant was introduced for characterization of the fatigue properties of brittle structural films. A ~3 μm square hole was added to the center of the remaining ligament of a notched cantilever beam in order to blunt the crack and, under resonant loading, to halt motion of the structure. Figure 3 shows scanning electron micrographs of single- and double-notched specimens with centrally located holes. The polycrystalline germanium sacrificial layer was removed using 50% H_2O_2 for 1.5 hours followed by drying at 110°C in air for 2 minutes. The structures were excited near the natural frequency of the uncracked structure and the amplitude of the electrostatic excitation was rapidly increased until the structure ceased to resonate. After testing, the structures were examined in the SEM, without the use of conductive coatings typically employed to improve image contrast of low conductivity materials.

2.2. Numerical modeling

A series of planar, finite element models were evaluated using a commercial software package (ANSYS v. 5.7). Modal and quasi-static structural analyses of the uncracked structure were used to determine the dynamic response of the structure and the applied stress amplitude for a given displacement of the structure. The fatigue characterization structure was modeled as an elastically isotropic, notched, cantilever beam and mass, with the geometry determined by SEM of released devices, as summarized in Figure 1. Six-node, triangular, plane-stress, solid elements with constant thickness were used in the model and small elastic deformations were assumed. The displacements of nodes located at the base of the notched cantilever beam were set to zero to achieve the "built-in" boundary conditions of the structure. The mesh in the vicinity of the notch was refined until solutions converged. An average of the Voigt and Reuss bounds for a random, polycrystalline silicon aggregate (Young's modulus, E = 163 GPa, Poisson's ratio, ν = 0.23 (Simmons and Wang, 1971)) was used for the elastic properties of the elements. The density of the polycrystalline silicon in the modal analysis was assumed to be the same as the bulk, single crystal form (ρ = 2329 kg/m^3 (Tatsumi and Ohsake, 1988)). A subspace extraction method was used to determine the eigenvalues and eigenvectors for the system, establishing the first in-plane natural frequency of the structure. An identical, plane-stress model with unit thickness was used to establish the degree of non-ideality (i.e., the deviation from a mass-spring system) of the structure. The maximum principal stress at the notch root, σ_1, and angular rotation of the structure, θ, about the

midpoint of the remaining ligament, (W - D), due to a unit force applied at the center of mass of the plate, were used to determine the relationship between angular rotation and maximum principal stress.

Modal and quasi-static structural analyses of cracked, notched, cantilever-beam structures were performed using the same material properties and finite element package. Akin to the uncracked structures, small deformations and elastic isotropy were assumed, displacements of nodes at the base of the cantilever structure were set to zero, and the material properties of an ideal polycrystalline silicon aggregate were used. The model of the fatigue structure, with a single crack located on the centerline of the notch perpendicular to the root of the notch, was constructed with six-node, triangular, plane-strain elements. The singularity at the crack tip was modeled with twelve circumferential, unskewed elements, 1/20 of the crack length in size. The remaining element size was refined until model convergence was achieved. As with the uncracked structure, a subspace extraction method was used to determine the eigenvalues and eigenvectors for the system, establishing the first in-plane natural frequency of the structure. Structural analyses of the cracked structure were performed using six-node triangular plane-stress elements with thickness equal to that of the structure in a configuration that was otherwise identical to the models used for the modal analyses. A unit force was applied at the center of mass of the plate and the resulting angular rotation used to establish the specimen rotational compliance ($s_\theta = 1/k_\theta$). The stress intensity was then calculated from the displacement field immediately behind the crack tip (Anderson, 1995; Broek, 1986). The size of the crack was gradually increased to establish the nondimensional compliance, sEt, and stress-intensity geometry function, $f(a/(W - D))$, for the cracked characterization structure using standard fracture-mechanics procedures (Anderson, 1995; Broek, 1986).

To evaluate the stability of cracks in this structure under the resonant loading conditions, a lumped model approach was used. The dynamic behavior of the system was modeled as a damped, forced, mass-spring oscillator that was driven at or near its natural frequency, f_0. The stiffness of the spring, k, and crack-driving force, K, were determined from fracture-mechanics solutions shown in Table 1 (after ref. (Tada, et al., 2000)) and the mass of the model system established by the geometry of the structure. The amplitude of motion and the associated driving force for crack advance were determined from the relationship between the amplitude and frequency of the excitation waveform and the damping characteristics and natural frequency of the system (e.g., ref. (French, 1971)), as detailed in the Appendix. The damping of the system was assumed to be proportional to the velocity of the mass in the system, as is typical of many simple systems.

Crack stability under resonant loading was evaluated by calculating the maximum stress intensity, $K_{max} = \Delta K/(1 - R)$, where ΔK is the stress-intensity range and R is the load ratio, for an applied force or moment amplitude. From the system compliance, the natural frequency of the resonator could then be determined. The crack was extended, lowering the natural frequency of the structure, but with the excitation frequency remaining unchanged. The new stress amplitude was determined using the revised structure compliance, thus permitting the associated crack-driving force to be calculated. The process of extending the crack and calculating the new stress amplitude was repeated to generate a plot of the driving force as a function of crack length. The effect of damping on the system was investigated by modifying the quality factor of the initial configuration, Q_0, as defined in the Appendix.

This general procedure was applied first using compliance and stress-intensity solutions in the literature for three common geometries summarized in Table 1: micron-scale, edge-cracked beam in bending (t = 2 μm, W = 19.5 μm), single-edge-cracked plate in tension (t = 2 μm, W = 10 μm, L = 20 μm), and center-cracked plate in tension (t = 2 μm, W = 5 μm, L = 20 μm), where t is the thickness, W is the width, and L is the length of the specimen. The edge-cracked beam in bending was attached to a mass with a mass-polar moment of inertia the same as the mass in the structure shown in Figure 1 ($J_0 = 1.024\times10^{-17}$ kg·m^2), giving an initial natural frequency of 96.2 kHz. Similarly, the edge-cracked and center-cracked plates in tension were modeled with a 4.1288×10^{-5} kg mass that gave an initial natural frequency of 14.1 kHz and 10 kHz respectively. In a gravitational field, this corresponded to a tensile preload of ~20 MPa, a small fraction of the strength of silicon structural films (3-5 GPa (Greek, et al., 1999; Greek, et al., 1997; Kapels, et al., 1999; Sharpe, et al., 1998; Sharpe, et al., 1999; Tsuchiya, et al., 1997; Tsuchiya, et al., 1998)). The lumped model was then applied to the notched cantilever-beam fatigue structure (Figure 1). The finite element results were used for evaluating the compliance and stress-intensity factors. The mass polar moment of inertia, J_0, of the micromechanical fatigue characterization structure was calculated from the geometry of the plate and found to be 1.024×10^{-17} kg·m^2. This mass-spring system model corresponds to an initial natural frequency of ~43.5 kHz.

The finite element and lumped-parameter dynamic models were applied to experimental results from previously reported stress-life fatigue data (Muhlstein, et al., 2001a). The linear relationship between the maximum principal stress, σ_1, and the angular rotation of the structure provided the basis for determining the nominal stress from the experimentally measured angular rotation. The dynamic model of the structure was then utilized to evaluate the crack-growth rates in the structure using the following procedure. The measured natural frequency of the structure, f_{crack}, was normalized with respect to the initial natural frequency of the structure, f_0. A linear interpolation of the normalized natural frequency as a function or normalized crack length, $a/(W - D)$, developed from the dynamic model was used to determine the crack length as a function of time. The maximum stress intensity immediately prior to failure was taken as an estimate of the fracture toughness of the material.

3. Results

3.1. Resonant-loaded beams with holes

Polycrystalline silicon-germanium fatigue characterization structures similar in geometry to Figure 1 were excited with continuously increasing stress amplitude at a fixed frequency in laboratory air until motion ceased. Observation of the single and double-notched beams with centrally located holes using the scanning electron microscope revealed cracks emanating from the root of the notch that terminated at the hole, as shown in Figure 3.

3.2. Dynamic and quasi-static finite element analyses

The dynamic and quasi-static behavior of the uncracked fatigue characterization structure was evaluated using the finite element methods described above. The first in-plane natural frequency of the structure, f_0, was extracted from the finite element models and the mode-

shape evaluated by inspection of the exaggerated displacements. The natural frequency of the uncracked structure was found to be 43,217 kHz for both the full (t=1.97 μm) and unit thickness plane-stress modes. The torsional stiffness, k_θ, of the uncracked structure due to a unit force applied at the center of mass of the toroidal plate was found to be 7.6605×10^{-7} N·m/rad. When k_θ is combined with the calculated mass polar moment of inertia, the natural frequency of the mass-spring system is calculated to be 43,531 kHz. The maximum principal stress at the root of the notch due to a unit force applied at the center of mass was linearly related to the angular rotation of the mass (1.0107×10^{11} Pa/rad). The spatial distribution of the stresses along the centerline of the notch was extracted from the finite element solution. The spatial distribution of the stresses in the notched cantilever beam are shown in Figure 4(a) where the principal stress, σ_1, is normalized by the outer fiber principal stress in the beam remote from the notch, $\sigma_{1,\infty}$, and the distance from the notch root, r, is normalized by the remaining ligament size, (W - D). The calculated stress concentration factor, K_t, was found to be 2.03. The maximum principal stress along the centerline of the notch decreases as $1/r^2$ for $r/(W - D) < 0.1$, as shown by the curve fit in Figure 4(b). The solutions from Noda (Noda, et al., 1995) have been used previously to define the stress amplitude applied during stress-life testing (Muhlstein, et al., 2001b).

Similar to the previous case, the dynamic behavior of the cracked fatigue characterization structure was also evaluated using finite element methods. The first in-plane natural frequency of the cracked structure, f_{crack}, was extracted from the model and the mode-shape evaluated by inspection of the exaggerated displacements. The relationship between normalized crack length ($a/(W - D)$) and normalized natural frequency (f_{crack}/f_0) for the plane-stress model is shown in Figure 5 and fit to the ninth-order polynomial shown in Table 2. Although the relationship is nonlinear, in the early stages of crack growth a ~1 Hz change in natural frequency corresponds to ~1 nm of crack extension. Interpolation methods should be used when calculating small, normalized crack lengths, i.e., $a/(W - D) < 0.01$, since the quality of the curve fit in this range is poor.

Standard fracture-mechanics analyses were used to determine the compliance, s, and stress-intensity factor, K, for the cracked fatigue characterization structure from the plane-strain finite element model detailed in the previous section. The compliance of the cracked structure for a given crack length was determined from the displacement of the center of mass of the toroidal plate due to a unit force applied at the center of mass. The equivalent angular rotation of the plate about the midpoint of the remaining ligament of the beam was determined from the geometry of the structure. From general analytical solutions, it is known that the crack-tip stresses and strains are proportional to the linear-elastic crack parameter, K, and have a general functional form dependent on the mode of loading (Anderson, 1995; Broek, 1986). Thus, the location of, and stresses (or displacements) at, nodes near the crack tip can be used to calculate K for a given applied force. This strategy was used to calculate K as a function of crack length for a unit applied force at the center of mass of the toroidal plate. The results of the compliance and stress-intensity factor analyses were then recast in the standard functional forms used in fracture mechanics. The compliance results are shown in the standard, nondimensional compliance form ($sEt = S(a/W)$) (Anderson, 1995; Broek, 1986) in Figure 6 and fit with the ninth-order polynomial shown in Table 2. Similarly, the geometric function, $f(a/(W - D))$ (Anderson, 1995; Broek, 1986), for the stress-intensity factor

($K = \sigma\sqrt{\pi \cdot a} \cdot f\left(a/(W-D)\right)$) of the cracked, notched, cantilever-beam structure was determined (Figure 7) and fit to a ninth-order polynomial shown in Table 2.

3.3. Lumped dynamic model

The lumped dynamic model described in section 2.2 was applied to the three, micron-scale, resonant fatigue characterization structures, namely the edge-cracked plate in bending, single edge-cracked plate in tension, and center-cracked plate in tension; the calculated normalized crack-tip parameters, as a function of normalized crack length and quality factor, are shown in Figure 8. The model was also applied to the cracked, notched cantilever-beam fatigue characterization structure (Fig. 1) using the fracture-mechanics solutions derived above. Results are shown in Figure 9, where the driving force for crack advance is presented as a function of crack length and quality factor.

3.4. Stress-Life (S-N) Fatigue Data Analysis

Previously, 28 polycrystalline silicon specimens were tested to failure in laboratory air (Muhlstein, et al., 2001a). The fatigue lives ranged from 28 fatigue specimens tested in room air; lives, N_f, varied from ~10 sec to 34 days (3×10^5 to 1.2×10^{11} cycles) over an angular rotation amplitude, θ, of ~0.02 to 0.04 radians at R = -1. The silicon films displayed "metal-like" *S-N* behavior, with an endurance strength at 10^9 - 10^{10} cycles of roughly half the (single-cycle) fracture strength. The relationship between angular rotation and maximum principal stress determined using the finite element model was used to calculate the applied stress amplitude which ranged from ~2.2 to 4.4 GPa (Figure 10). For each specimen, the crack length as a function of accumulated cycles was determined from a linear interpolation of the finite element model-derived relationships between natural frequency and crack length shown in Figure 5. A representative result of the calculated crack length as a function of time is shown in Figure 11. The final crack length measured immediately prior to failure, a_f, from the normalized natural frequency for the specimens in Figure 10 is shown as a function of specimen life, N_f, in Figure 12. The applied stress amplitude for a given test and the crack size just prior to failure were used to estimate the fracture toughness of the material, K_c (Figure 13). For the thin-film polysilicon fatigue tests, critical crack sizes were observed to range from ~5.5 to 66 nm depending on the applied stress amplitude. The average fracture toughness measured by this technique for failure of the polycrystalline silicon films was 0.85 MPa√m.

4. Discussion

The finite element and numerical models provide important insight into the dynamic behavior of crack-free structures and the stresses in the vicinity of the notched beam fatigue characterization specimens. Similarly, the models of the cracked structure can be used to determine the size and stability of cracks, as well as the fracture toughness of the material. The purpose of this section is to discuss the implications of the models for the behavior of the structure and the fatigue resistance of polycrystalline silicon.

Comparison of the various models of the dynamic behavior of the crack-free characterization structure provides useful insight into the behavior of the structure. The agreement between the first in-plane natural frequency predicted by the unit and full-thickness finite element models of the fatigue characterization structure and the 0.7% difference between the plane-stress finite element and the mass-spring description establish that the use of a mass-spring idealization is reasonable. However, there is a marked difference between the predicted natural frequency of the plane-stress model (43,217 Hz) and what is typically observed experimentally (41,693 Hz) (Muhlstein, et al., 2001a). Since the stiffness of the structure is proportional to the elastic modulus, the experimentally observed Young's modulus *appears* to be about 152 GPa, i.e., some 7% below the ideal polycrystalline value. It is believed that this is not an anomalously low elastic modulus, but rather arises from the compliance of the "anchor" at the base of the cantilever structure (Van Arsdell, 1997). Specifically, the use of idealized, polycrystalline aggregate elastic properties and perfectly clamped boundary conditions provide a conservative estimate of the applied stress amplitudes during *S*/*N* fatigue testing. While the built-in assumption for the base of the fatigue characterization structure may introduce up to a 7% error in the calculated stress amplitude, the general trends observed in *S*/*N* and dynamic behavior should be faithfully represented. Maximum principal stresses at the root of the notch, determined from the plane-stress finite element model of the crack-free fatigue characterization structure, gave values proportional to the angular rotation of the resonant mass (1.0107×10^{11} Pa/rad). The stress field falls off at a rate proportional to $1/r^2$, and the notch the effects are most important for $r/(W - D) < 0.1$ (within 0.65 μm of the root) as shown in Figure 4(b). General solutions for V-shaped notches in flat plates loaded in bending, developed by Noda (Noda, et al., 1995), give a K_t value of 2.03 for the present notched cantilever beam, which compares favorably with the finite element solutions in the present study and the simplified (beam-only) models used previously (Muhlstein, et al., 2001a). While the understanding of the notch stress distribution and dynamic behavior of the structure are important, the behavior of cracked fatigue characterization structures is particularly useful.

The interaction between natural frequency of a cracked structure and the excitation frequency, depicted schematically in Figure 2, was observed experimentally as a loss of resonance in the hole specimens. If a fatigue crack is allowed to propagate into a hole under the correct loading conditions (De Rijk, 1970; Van Leeuwen, 1970; Van Oosten Slingeland and Broek, 1973), the crack-tip tip radius is effectively "blunted", in the present case from Ångstroms to micrometers, which can lead to arrest. Because the natural frequency of the structure has been radically reduced, during the next electrostatic cycle the structure is not excited at resonance since the frequency of the impulse has remained unchanged. This provides a "graceful" failure mode that prevents shorting of the electrostatic actuator when the specimen separates. More importantly, this is not the only way to decrease the driving force for crack advance under resonant loading conditions.

In general, under nominally linear-elastic conditions, when a constant force is applied normal to the crack plane (i.e., mode I loading), an increasing *K*-gradient results and stable crack growth is not observed in materials that do not exhibit resistance-curve behavior (Anderson, 1995; Broek, 1986; Lawn, 1993). In contrast, a mode I crack subjected to a constant displacement will usually be subjected to a decreasing *K*-gradient and stable crack propagation can occur once the applied driving force reaches the critical stress intensity, K_c.

Creative mechanical design can lead to exceptions to these general trends (e.g., (Fitzgerald, et al., 1999; Gonzalez and Pantano, 1990)) just as rapidly varying the applied force or displacement can, in principle, be used to generate the desired crack-tip driving force and K-gradient. The applied stress-intensity range, ΔK, gives the analogous driving force for fatigue-crack growth in linear elastic solids. Fatigue cracks subjected to increasing ΔK gradients ($d\Delta K/da$) accelerate while decreasing gradients eventually lead to crack arrest. The resonant loading conditions encountered in micromechanical fatigue testing play an important role in the stability of cracks in these structures.

If a micromechanical fatigue system is modeled as a damped, forced, mass-spring oscillator that is driven at or near its natural frequency, the stiffness and crack-driving force of the "spring" can be determined from fracture-mechanics solutions that describe the geometry of the specimen. A wide variety of solutions are summarized in handbooks, e.g. (Tada, et al., 2000). The amplitude of motion can be determined from the relationship between the amplitude and frequency of the excitation waveform and the damping characteristics and natural frequency of the system. This general approach allows the evaluation of fatigue crack stability for a wide variety of configurations and reflects the behavior of a variety of mechanical testing structures used to characterize structural films used in MEMS. If the system is driven at or near the natural frequency of the crack-free structure, the unique loading conditions depicted schematically in Figure 2 may develop. A structure excited at f_0 will begin at an amplitude of motion as defined by Eq. A2 in the Appendix. As the crack advances, the natural frequency of the structure decreases. Since the excitation frequency has remained unchanged, the amplitude of motion decreases as the coupling between the structure and excitation force is reduced. If the rate of load shedding is sufficiently rapid (i.e., high enough Q), a decreasing ΔK gradient may develop. What would seem at first glance to be a force-controlled configuration is actually limited by the change in stiffness of the structure. In the case of the micromechanical resonators for fatigue characterization, these force-controlled, displacement-limited conditions may develop when the damping in the system is altered by lowering the ambient pressure of the surrounding environment.

As noted above, the mode I compliance and stress-intensity factor solutions for edge and center-cracked plates in tension and edge-cracked beams in bending from (Tada, et al., 2000) were used as test cases for the general model of crack stability under fatigue loading. In heavily damped (i.e., low Q) systems, the stress amplitude does not significantly change as the crack advances into the material and the loading conditions are not unlike constant force or moment conditions. The crack grows into an increasing ΔK gradient and will accelerate and eventually fail when K_{max} reaches the fracture toughness, K_c, of the material (i.e., is unstable). However, as the level of damping is reduced the driving force, ΔK, and its gradient change significantly; the lower damping in the system leads to a rapid decrease in the applied stress amplitude as the crack advances. Once the quality factor reaches relatively high values (in excess of 1000), the gradient is such that the fatigue crack is decelerating and will eventually arrest (i.e., is stable). This phenomenon is quite general, and is observed with both edge and centrally located cracks loaded in tension or bending.

The stability of cracks in the actual fatigue characterization structure is shown as a function of system damping in Figure 9. The behavior of the structure is similar to the model systems based on edge and center-cracked plates in tension and edge-cracked beams in bending fracture-mechanics solutions from (Tada, et al., 2000). Reducing the system

damping can create decreasing driving forces and driving force gradients for crack advance. This is pertinent where fatigue testing is required for different environments. For the case of the fatigue characterization structure used in thin-film silicon research, Q changes from about 100 to more than 1000 when the environment is changed from room air at atmospheric pressure to a vacuum of 10^{-6} Torr. Consequently, one would expect the *mechanical loading* (as well as the environmental) conditions to be significantly different for tests in these two environments.

Controlled environment testing is used to probe the role of environment in fracture and fatigue processes. Normally, testing in vacuum is a convenient and effective means of limiting environmental effects. However, these model results show that altering the damping conditions of a micromechanical resonator can have a dramatic effect on the driving force on and stability of fatigue cracks. Specifically, cracks that would be unstable at atmospheric pressure may arrest *in vacuo*. Furthermore, incremental, unstable crack advance could be mistaken for subcritical fatigue-crack growth when the excitation frequency is periodically updated during a micromechanical fatigue test conducted in vacuum.

One should note that analyses of resonant fatigue systems are limited by the ability to model adequately the loading conditions and by the behavior of the system as the crack becomes an appreciable fraction of the specimen. For example, the inhomogeneous distribution of stress in macroscopic resonant fatigue specimens complicates the evaluation of the stress-intensity factor (Schoeck, 1982). Fortunately, this is not a problem in the mass-spring systems used in micromechanical fatigue structures. However, in both continuous and mass-spring systems the load ratio of -1 is problematic, as the opposing faces of the crack come into contact during the compression portion of the loading cycle (and even earlier if crack-closure phenomena are active). In this study, as with most fracture-mechanics analyses, this problem is alleviated by computing the stress intensity in terms of the tensile portion of the cycle only; for this reason, the driving force results are presented in terms of K_{max}. Additionally, at long crack lengths the difference in compliance during the opening and closing portions of the loading cycle introduces significant nonlinearity in the cracked mass-spring oscillator. Furthermore, out-of-plane bending and torsional modes tend to couple with the in-plane bending mode at large normalized crack lengths (Van Arsdell, 1997). These factors can limit the range of applicability of the lumped model and finite element results. Fortunately, cracks observed in the micromechanical fatigue characterization structure modeled here are usually very short (e.g., with $a/(W - D) << 0.1$), such that these limitations are insignificant.

When the finite element and lumped models are used to interpret the stress-life fatigue behavior of polysilicon, a variety of important observations can be made. If the damage accumulation (i.e., the decrease in resonant frequency) during the fatigue test is assumed to be due to the formation of a crack, the crack length can be readily determined as a function of time (Figure 11). While this is a simplification of the fatigue degradation process, experimental observations of cracks in structures are consistent with the observed changes in natural frequency (Muhlstein, et al., 2001c; Muhlstein, et al., 2001d). The crack-growth behavior determined from the change in natural frequency of the specimen (Figure 11) suggests that the crack-growth rates are decreasing as the crack advances. This behavior has been observed for microstructurally-small cracks, cracks growing under displacement control, cracks growing into residual stress fields, and cracks approaching interfaces. In the present

case, the effect is likely related to several of these factors acting *in concert*, as detailed in (Muhlstein, et al., 2001c). If the crack-driving force at failure is taken as an estimate of the fracture toughness, the toughness of the material can be determined. The crack length estimates at failure were used with plane-strain models of the stress intensity for the notched cantilever beam structure. Results from the polysilicon fatigue tests (Figure 13) give an average fracture toughness of ~0.85 MPa√m, with critical crack sizes in the range ~5.5 to 66 nm depending on the applied stress amplitude. As prior studies (Muhlstein, et al., 2001c; Muhlstein, et al., 2001d) have indicated that the oxide thickness at the notch is on the order of 100 nm, it is clear that the crack initiation, growth and final (overload) processes during thin-film silicon fatigue all occur within the native oxide. The measured toughness value of ~0.85 MPa√m is thus indicative of the fracture toughness of the amorphous silica reaction layer.

5. Conclusions

Based on experimental and numerical analyses of resonating micromechanical fatigue structures used in micron-scale testing of structural silicon films, which incorporate experimental observation and finite element (quasi-static and dynamic) and lumped dynamic models, the following conclusions may be made:

1. The notched cantilever-beam fatigue characterization structure behaves as a lumped mass-spring oscillator (within 0.7%). The idealized clamped boundary conditions for the structure introduce error of ~7% to the maximum principal stress at the root of the notch through the estimate of the specimen compliance.
2. The notch of the fatigue characterization structure influences the compliance and stress-intensity factor solutions for the notched cantilever beam. The influence of the notch stress field falls off at a rate proportional to $1/r^2$, and the effects of the notch are most important within 0.65 μm of the root (i.e., $a/(W - D) < 0.1$). This corresponds to the range of crack lengths generally of interest for stress-life fatigue characterization in micron-scale structures made from brittle materials.
3. The dynamic response of the fatigue characterization structure is extremely sensitive to crack length. Although the relationship is nonlinear, a 1 nm extension in crack length corresponds to ~1 Hz change in natural frequency.
4. The presence of a centrally located hole in notched micromechanical fatigue characterization structures prevents complete separation of the test specimen by blunting the crack when the resonator is driven at a fixed excitation frequency.
5. Fatigue crack stability in micromechanical resonators driven at a constant frequency at or near the natural frequency of the system is a function of the damping characteristics of the system. Specimens in micromechanical fatigue characterization structures are subjected to force-controlled, displacement-limited loading conditions. Lowering the damping in the system, e.g., by testing *in vacuo*, can lead to crack arrest from purely mechanical factors. This effect must be considered in the evaluation of results from controlled environment testing using this test geometry.

6. Fatigue lives measured using micromechanical fatigue resonators *in vacuo* cannot be directly compared to atmospheric pressure data due to differences in the gradient of the applied stress-intensity range. Indeed, fatigue testing in low-pressure environments may give the anomalous appearance of subcritical crack growth in the absence of fatigue degradation.
7. During the fatigue of thin-film polysilicon, critical crack sizes were observed to range from ~5.5 to 66 nm depending on the applied stress amplitude; average toughness values were found to be 0.85 MPa√m. These results, together with previous studies, suggest that the processes of crack initiation, growth and final overload failure all occur within the native oxide layer.

Acknowledgements

This work was funded by the Director, Office of Science, Office of Basic Energy Research, Materials Sciences Division of the U.S. Department of Energy under Contract No. DE-AC03-76SF00098 (for R.O.R.). The authors wish to thank Dr. S. B. Brown for his prior support, Dr. W. Van Arsdell for the original specimen design, and Dr. J. M. McNaney for helpful discussions.

Appendix: Forced, Damped, Mass-Spring System Equations of Motion

In contrast to the systems used for macroscopic ultrasonic fatigue testing, most micromechanical fatigue characterization structures can be modeled as forced, damped, mass-spring oscillators (e.g., (Van Arsdell, 1997; Van Arsdell and Brown, 1999)). The deformation of the structure is localized to the test specimen and the attached mass, m, reduces the natural frequency, f_0, of the system. If we assume that the damping in the system is proportional to the velocity of the mass, $\mathrm{d}x/\mathrm{d}t$, and the stiffness of the specimen is given by k, the motion of the system may be described by the following second-order differential equation:

$$\begin{aligned} &\frac{\mathrm{d}^2 x}{\mathrm{d}t^2} + \gamma \frac{\mathrm{d}x}{\mathrm{d}t} + f_0^2 x = \frac{F_0}{m}\cos(f \cdot t) \quad , \\ &\frac{k}{m} = f_0^2 \quad , \\ &\frac{b}{m} = \gamma \quad , \end{aligned} \tag{A1}$$

where x is the position of the center of mass at time, t, and f is the frequency of the applied force, F_0. The damping parameter, γ, is the ratio of the velocity-dependent resistive force, b, to the mass. Solutions to this equation are routinely derived in introductory texts on dynamics (e.g., (French, 1971)). It is convenient to introduce the quality factor, $Q = f_0/\gamma$, as a measure of the damping characteristics of the system. With this added notation, the solution of the amplitude of motion as a function of excitation frequency, $A(f)$, is given by:

$$A(f) = \frac{\frac{F_0}{m}}{\left[(f_0^2 - f^2) + \left(\frac{f \cdot f_0}{Q} \right)^2 \right]^{1/2}} \quad . \tag{A2}$$

For rotational systems, e.g., where the angular rotation is a function of an applied moment, the rotational stiffness, k_θ, and the mass polar moment of inertia, J_θ, are used to describe the stiffness and mass of the system, respectively.

References

Allameh, S.M., Gally, B., Brown, S., Soboyejo, W.O., 2000. On the evolution of surface morphology of polysilicon MEMS structures during fatigue. In: Kahn, H., de Boer, M., Judy, M., Spearing, S.M. (Eds.), Materials Science of Microelectromechanical System (MEMS) Devices III. Boston, MA, pp. EE2.3.1-EE2.3.6.

Anderson, T.L., 1995. Fracture mechanics: Fundamentals and Applications, 2nd ed. CRC Press, Boca Raton.

Ballarini, R., Mullen, R.L., Yin, Y., Kahn, H., Stemmer, S., Heuer, A.H., 1997. The fracture toughness of polysilicon microdevices: a first report. Adv. Appl. Mech. 12, 915-922.

Broek, D., 1986. Elementary engineering fracture mechanics, 4th ed. Martinus Nijhoff; Distributed by Kluwer, Dordrecht; Boston: Hingham, MA.

Brown, S.B., Van Arsdell, W., Muhlstein, C.L., 1997. Materials reliability in MEMS devices. In: Senturia, S. (Ed.), Proceedings of International Solid State Sensors and Actuators Conference (Transducers '97). Chicago, IL, USA, pp. 591-593.

Chati, M., Rand, R., Mukherjee, S., 1997. Modal analysis of a cracked beam. J. Sound Vibr. 207, 249-270.

Chen, C.P., Leipold, M.H., 1980. Fracture toughness of silicon. Amer. Cer. Soc. Bull. 59, 469-472.

Chondros, T.G., Dimarogonas, A.D., Yao, J., 1998. A continuous cracked beam vibration theory. J. Sound Vibr. 215, 17-34.

De Rijk, P., 1970. Empirical investigation on some methods for stopping the growth of fatigue cracks, TR 70021, National Aerospace Institute.

Fitzgerald, A.M., Dauskardt, R.H., Kenny, T.W., 1999. Fracture toughness and crack growth phenomena of plasma-etched single crystal silicon. Sens. Actuators A A83, 194-199.

Franke, A.E., Jiao, Y., Wu, M.T., King, T.J., Howe, R.T., 2000. Post-CMOS modular integration of poly-SiGe microstructures using poly-Ge sacrificial layers., Solid-State Sensor and Actuator Workshop (TRF Cat. No.00TRF-0001) Technical Digest. Solid-State Sensor and Actuator Workshop. Hilton Head Island, SC, USA, pp. 18-21.

French, A.P., 1971. Vibrations and waves. Norton, New York.

Gonzalez, A.C., Pantano, C.G., 1990. A compression-loaded double cantilever beam specimen. J. Am. Ceram. Soc. 73, 2534-2535.

Greek, S., Ericson, F., Johanasson, S., Furtsch, M., Rump, A., 1999. Mechanical characterization of thick polysilicon films: Young's modulus and fracture strength evaluated with microstructures. J. Micromech. Microeng. 9, 245-251.

Greek, S., Ericson, F., Johansson, S., Schweitz, J.A., 1997. In situ tensile strength measurement and Weibull analysis of thick film and thin film micromachined polysilicon structures. Thin Solid Films 292, 247-254.

Kahn, H., Ballarini, R., Mullen, R.L., Heuer, A.H., 1999a. Electrostatically actuated failure of microfabricated polysilicon fracture mechanics specimens. Proc. Roy. Soc. A 455, 3807-3823.

Kahn, H., Tayebi, N., Ballarini, R., Mullen, R.L., Heuer, A.H., 1999b. Fracture toughness of polysilicon MEMS devices., Transducers '99: 10th International Conference on Solid State Sensors and Actuators. Sendai, Japan, pp. 274-280.

Kapels, H., Aigner, R., Binder, J., 1999. Fracture strength and fatigue of polysilicon determined by a novel thermal actuator [MEMS]., Proceedings of the 29th European Solid-State Device Research Conference. Leuven, Belgium, pp. 1522-1528.

Lawn, B.R., 1993. Fracture of brittle solids, 2nd ed. Cambridge University Press, Cambridge, New York.

Mahmoud, M.A., Zaid, M.A., Harashani, S.A., 1999. Numerical frequency analysis of uniform beams with a transverse crack. Comm. Numer. Meth. Engin. 15, 709-715.

Mayer, H., 1999. Fatigue crack growth and threshold measurements at very high frequencies. Int. Mater. Rev. 44, 1-34.

McGuire, S.M., Fine, M.E., Achenbach, J.D., 1995. Crack detection by resonant frequency measurements. Metal. Mater. Trans. A 26A, 1123-1127.

Muhlstein, C.L., Brown, S.B., Ritchie, R.O., 2000. High cycle fatigue of polycrystalline silicon thin films in laboratory air. In: Kahn, H., de Boer, M., Judy, M., Spearing, S.M. (Eds.), Materials Science of Microelectromechanical System (MEMS) Devices III. Boston, MA, pp. EE5.8.1-EE5.8.6.

Muhlstein, C.L., Brown, S.B., Ritchie, R.O., 2001a. High-cycle fatigue and durability of polycrystalline silicon films in ambient air. Sens. Actuators A 94, 177-188.

Muhlstein, C.L., Brown, S.B., Ritchie, R.O., 2001b. High-cycle fatigue of single crystal silicon thin films. J. Micrelectromech. Sys. 10, 593-600.

Muhlstein, C.L., Stach, E.A., Ritchie, R.O., 2001c. High-Cycle Fatigue in Micron-Scale Structural Films of Polycrystalline Silicon: A Reaction-Layer Failure Mechanism. Acta Mater., submitted.

Muhlstein, C.L., Stach, E.A., Ritchie, R.O., 2001d. Mechanism of fatigue in micron-scale films of polycrystalline silicon for MEMS applications. Appl. Phys. Let., in press.

Noda, N.A., Sera, M., Takase, Y., 1995. Stress concentration factors for round and flat test specimens with notches. Int. J. Fat. 17, 163-178.

Ritchie, R.O., 1999. Mechanisms of fatigue-crack propagation in ductile and brittle solids. Int. J. Fract. 100, 55-83.

Schoeck, G., 1982. Calculation of the stress intensity in ultrasonic resonance. Z. Metall. 73, 576-578.

Sharpe, W.N., Brown, S., Johnson, G.C., Knauss, W., 1998. Round-Robin Tests of Modulus and Strength of Polysilicon. In: Brown, S., Gilbert, J., Guckel, H., Howe, R., Johnson, G., Krulevitch, P., Muhlstein, C. (Eds.), Microelectromechanical Structures for Materials Research. San Francisco, CA, pp. 57-65.

Sharpe, W.N., Turner, K.T., Jr., Edwards, R.L., 1999. Tensile testing of polysilicon. Exper. Mech. 39, 162-170.

Simmons, G., Wang, H., 1971. Single Crystal Elastic Constants and Calculated Aggregate Properties: a Handbook, 2nd ed. M.I.T. Press, Cambridge, MA.

St. John, C., 1975. The brittle-to-ductile transition in precleaved silicon single crystals. Phil. Mag., 1193-1212.

Stanzl-Tschegg, S., Mayer, H., 2001. In: Stanzl-Tschegg, S., Mayer, H. (Eds.), Proceedings of the International Conference on Fatigue in the Very High Cycle Regime. University of Agricultural Sciences, Vienna, Austria.

Suresh, S., 1998. Fatigue of Materials, 2nd ed. Cambridge University Press, Cambridge, England.

Tada, H., Paris, P.C., Irwin, G.R., 2000. The stress analysis of cracks handbook, 3rd ed. ASME Press, New York.

Tatsumi, Y., Ohsake, H., 1988., Properties of Silicon. IEE, London, UK. pp. 3-6.

Tsuchiya, T., Sakata, J., Taga, Y., 1997. Tensile strength and fracture toughness of surface micromachined polycrystalline silicon thin films prepared under various conditions. In: Cammarata, R.C., Nastasi, M., Busso, E.P., Oliver, W.C. (Eds.), Symposium Thin-Films-Stresses and Mechanical Properties VII. Symposium. Boston, MA, USA, pp. 285-290.

Tsuchiya, T., Tabata, O., Skakata, J., Taga, Y., 1998. Specimen Size Effect on Tensile Strength of Surface-Micromachined Polycrystalline Silicon Thin Films. J. Micrelectromech. Sys. 7, 106-113.

Van Arsdell, W., Ph.D., Massachusetts Institute of Technology, 1997.

Van Arsdell, W.W., Brown, S.B., 1999. Subcritical crack growth in silicon MEMS. J. Micrelectromech. Sys. 8, 319-327.

Van Leeuwen, H.P., 1970. The repair of fatigue cracks in low-alloy steel sheet, TR 70029, National Aerospace Institute.

Van Oosten Slingeland, G.L., Broek, D., 1973. Fatigue cracks approaching circular holes, Delft University.

Wong, B., Holbrook, R.J., 1987. Microindentation for fracture and stress-corrosion cracking studies in single-crystal silicon. J. Electrochem. Soc. 134, 2254-2256.

Yokoyama, T., Chen, M.C., 1998. Vibration analysis of edge-cracked beams using a line-spring model. Engin. Fract. Mech. 59, 402-409.

FIGURES

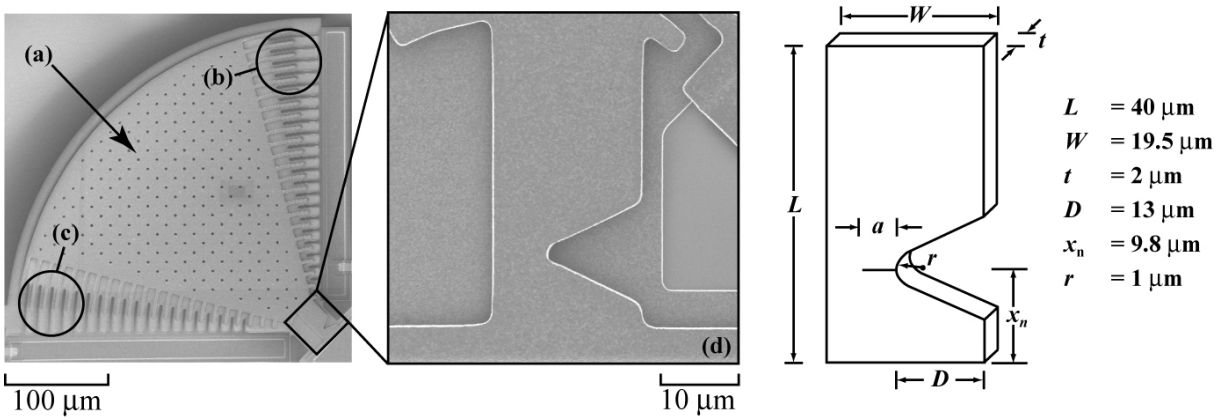

Figure 1. Scanning electron micrograph of the micron-scale fatigue characterization structure containing the notched cantilever-beam specimen used in this investigation. The (a) mass, (b) comb drive actuator, (c) capacitive displacement sensor, and (d) notched cantilever-beam specimen are shown. The nominal dimensions of the specimen are as indicated in the schematic.

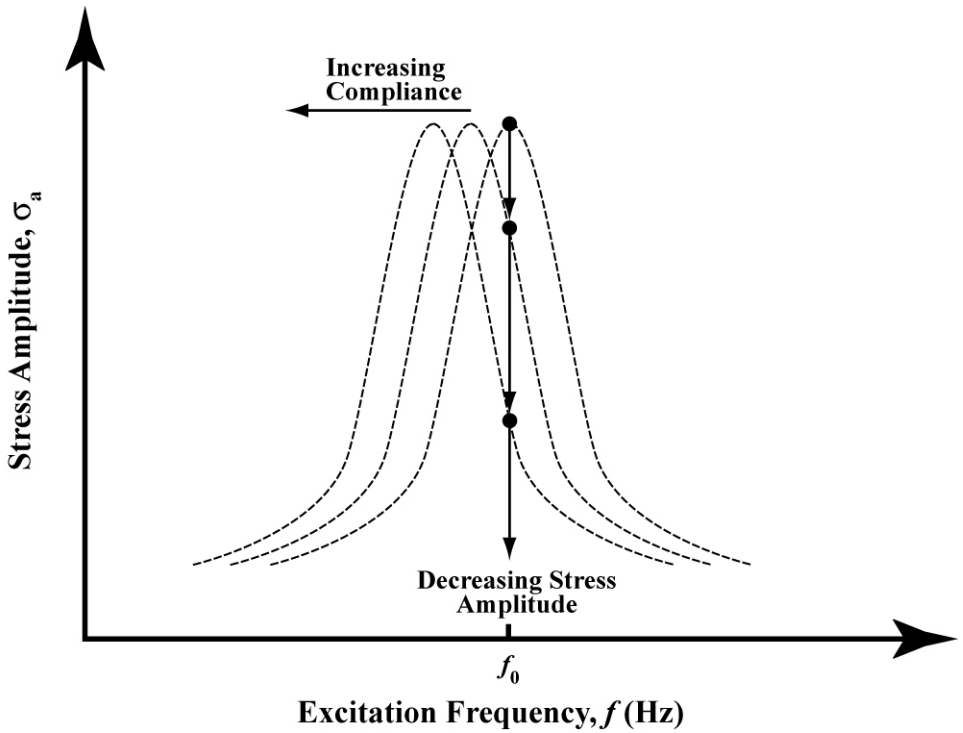

Figure 2. Schematic of the effect of increasing specimen compliance on the applied stress amplitude in a mass-spring system under loading at a fixed natural frequency. The dashed lines are the amplitude of stress (displacement) experienced by the simple harmonic oscillator as defined by Eq. A2 in the Appendix. The system is excited at the initial natural frequency of the undamaged system, f_0, but as damage accumulates the compliance increases. Depending on the damping in the system, the resonant-loaded structure can experience a significant reduction in the driving force for damage accumulation and crack advance.

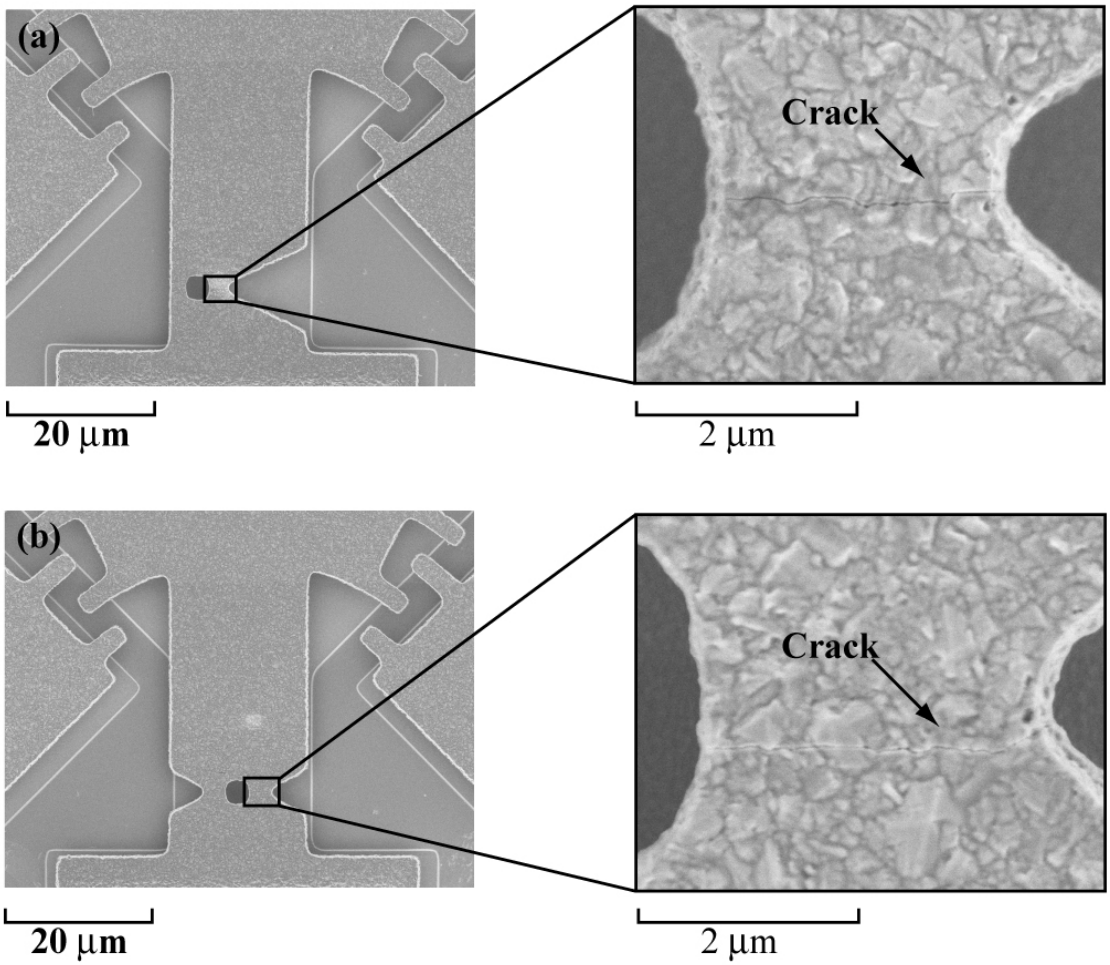

Figure 3. Scanning electron micrographs of (a) single and (b) double-notched cantilever-beam specimens in fatigue characterization structures with centrally located holes fabricated using a SiGe surface micromachining process (Franke, et al., 2000). The specimens were excited at a fixed natural frequency and the amplitude rapidly increased until motion of the structure ceased. Cracks initiated at the notch root and were arrested by the hole, preventing complete separation of the beam (insets), illustrating the interaction between the resonant loading conditions and crack advance in the structure.

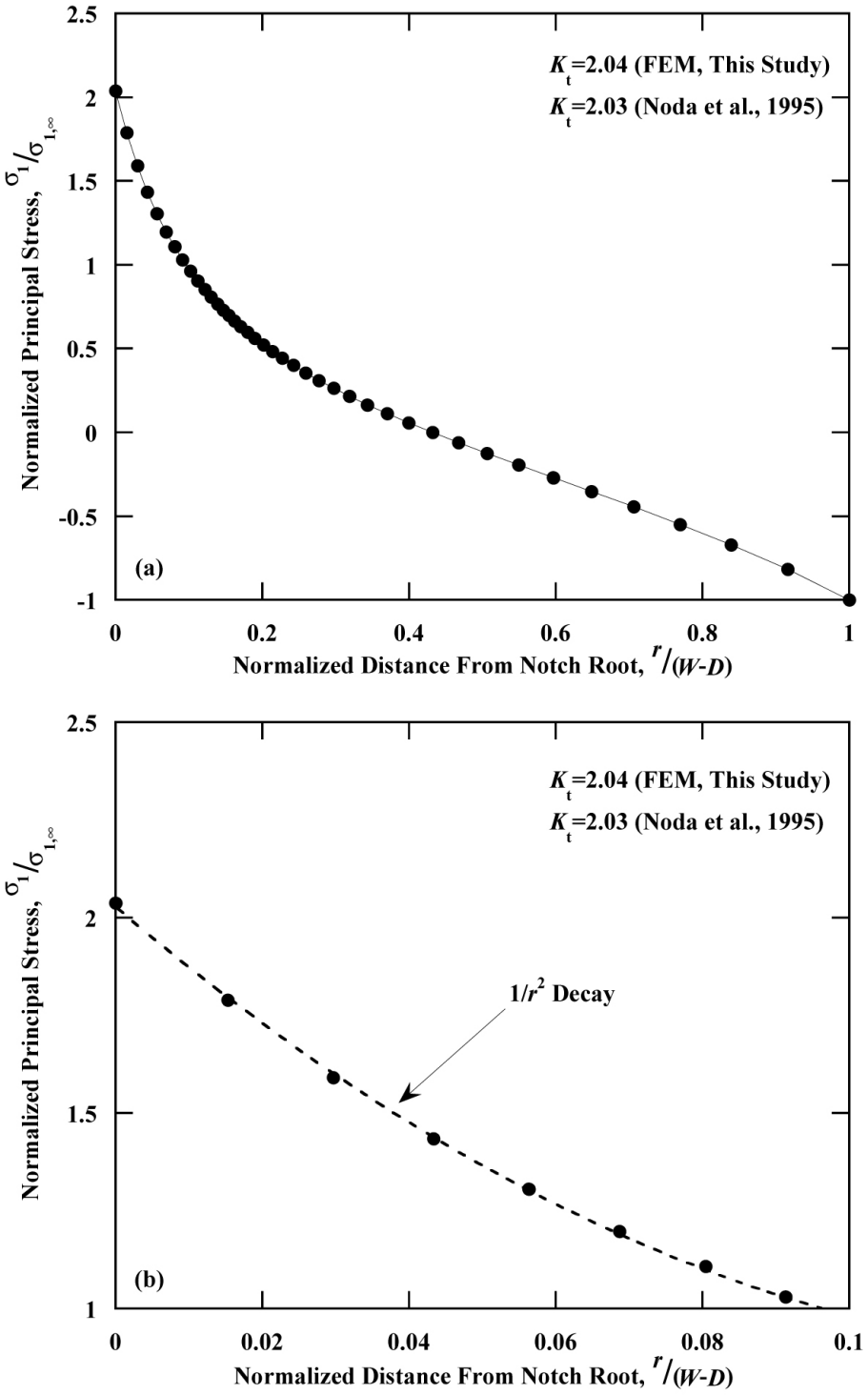

Figure 4. Stress-concentration effects of the notch in the cantilever beam in the fatigue characterization structure. (a) The normalized stress ($\sigma_1/\sigma_{1,\infty}$) at location, r, along the centerline of the notch is shown as a function of the remaining ligament (W - D) of the cantilever-beam structure. (b) The $1/r^2$ decay of the maximum principal stress near the root of the notch.

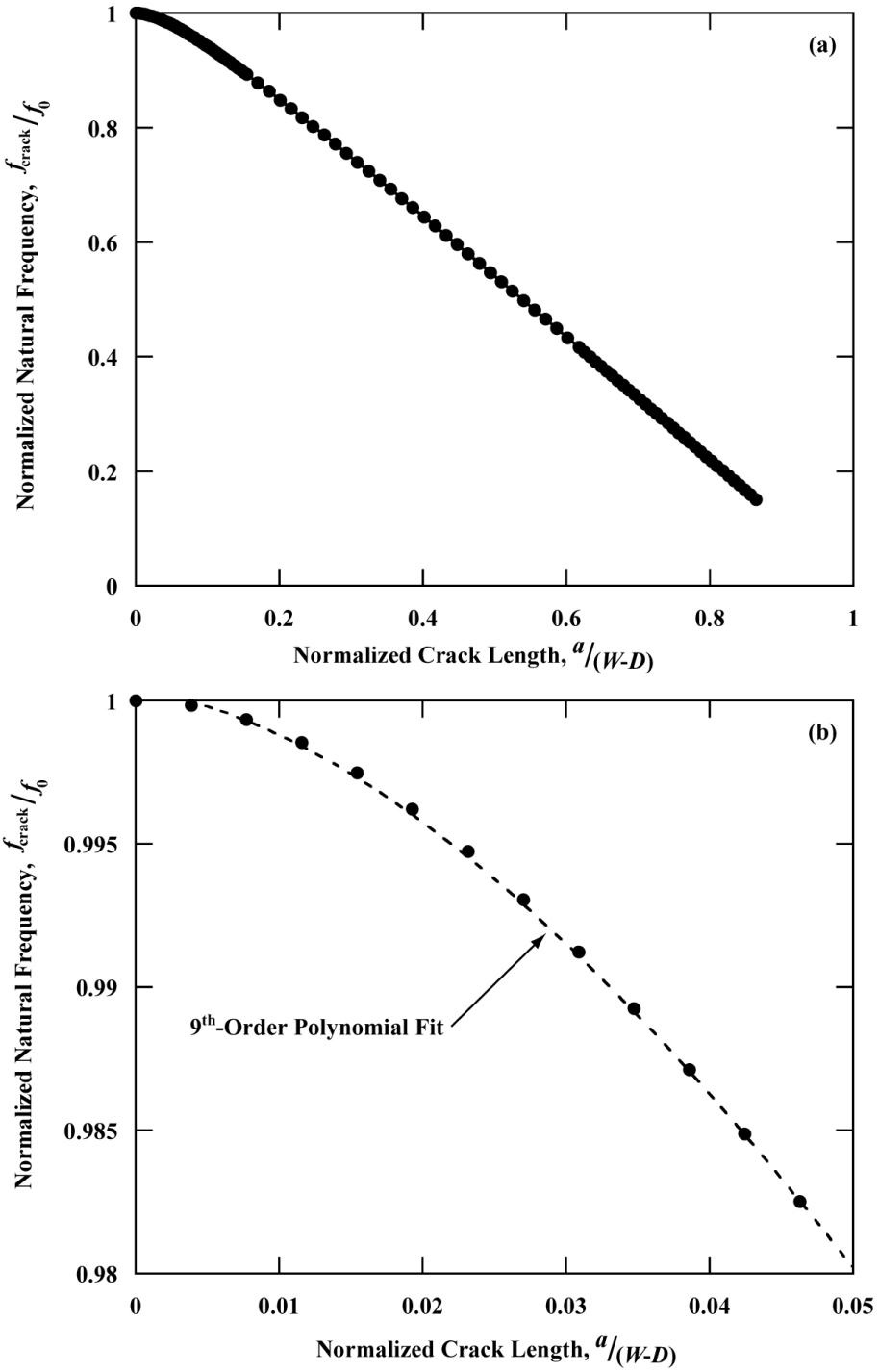

Figure 5. (a) The relationship between normalized crack length ($a/(W - D)$) and normalized natural frequency (f_{crack}/f_0) for the plane-stress (full thickness) finite element model of the notched cantilever beam in the fatigue characterization structure. (b) The behavior for small ($a/(W - D)$) and the associated ninth-order polynomial fit from Table 2 are shown.

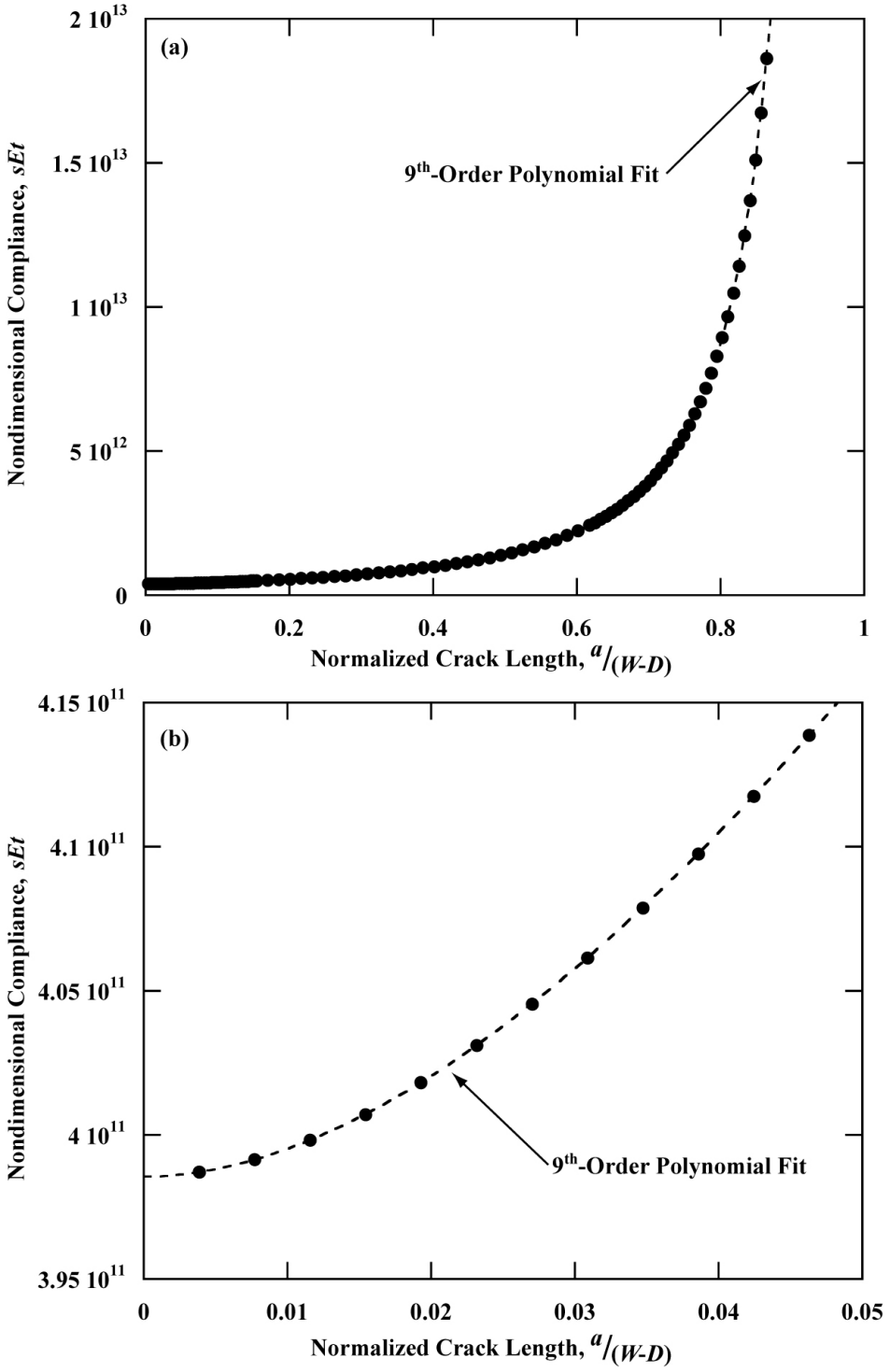

Figure 6. (a) The non-dimensional rotational compliance, $S(a/(W - D))=sEt$, of the cracked fatigue characterization structure due to a unit point load applied at the center of mass as a function of normalized crack length, $a/(W - D)$, determined from finite element methods. (b) The behavior for small ($a/(W - D)$) and the associated ninth-order polynomial fit from Table 2 are shown.

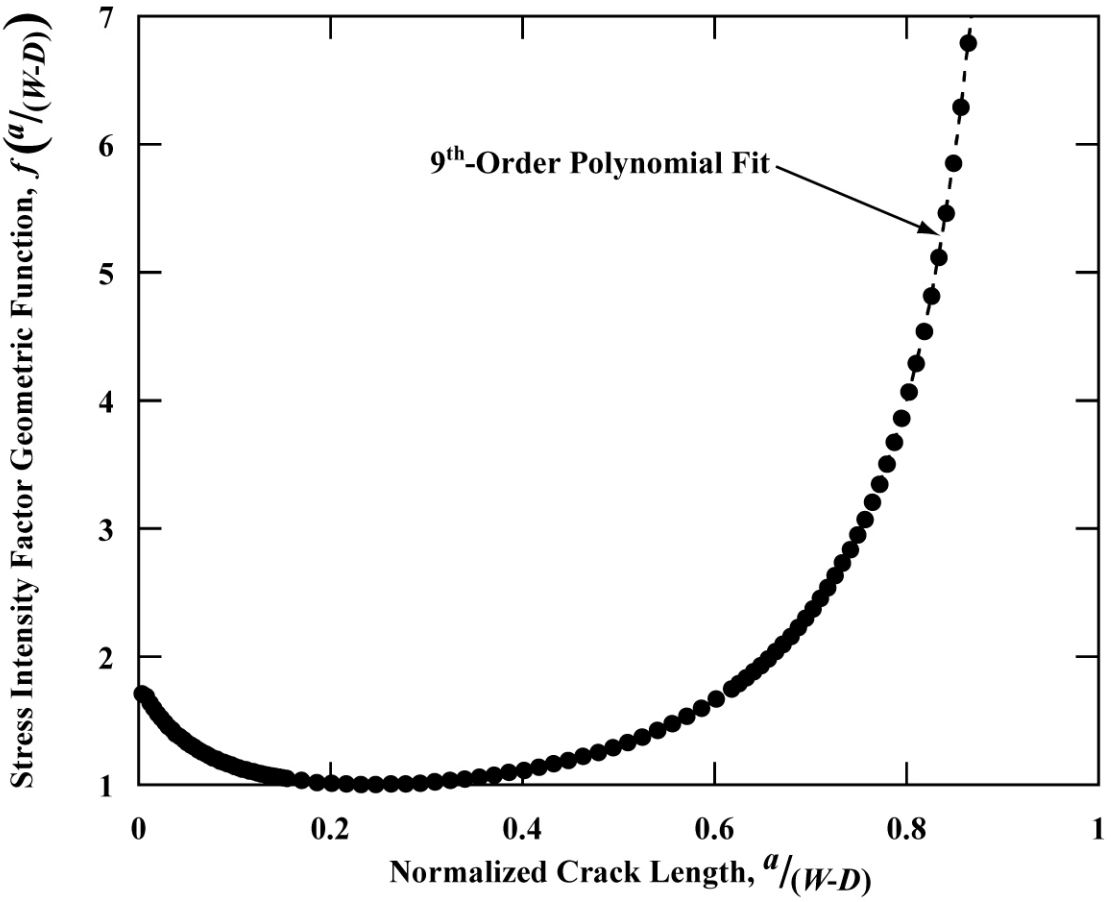

Figure 7. The geometric function, $f(a/(W - D))$, for the stress-intensity factor, $K = \sigma\sqrt{\pi \cdot a} \cdot f\left(a/(W-D)\right)$, of the cracked, notched, cantilever beam specimen within the fatigue characterization structure, determined from the displacement of nodes immediately behind the crack tip.

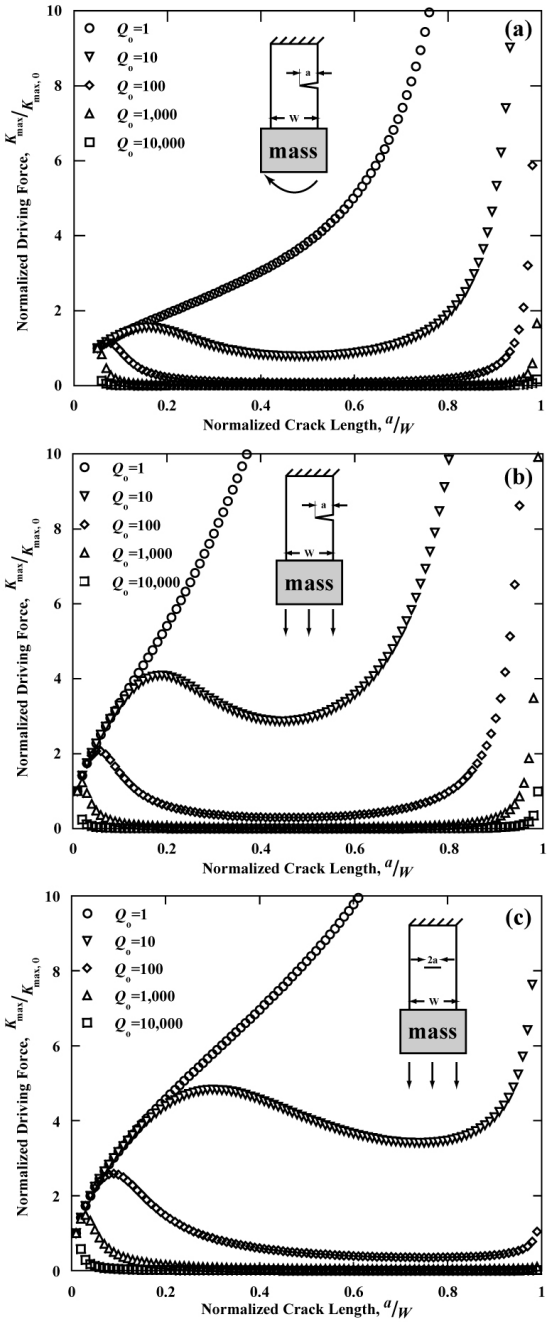

Figure 8. Stability of a fatigue crack in resonant-loaded fatigue characterization structures predicted by the lumped dynamic model. The normalized driving force for crack advance, $K_{max}/K_{max,0}$, as a function of normalized crack length, a/W, is shown for the (a) edge-cracked plate in bending, (b) edge-cracked plate in tension and (c) center-cracked plate in tension. In heavily damped systems (i.e. low Q_0), the fatigue crack will accelerate ($dK/d(a/W) > 0$). As the damping in the system is decreased (i.e. increasing Q_0), the crack will decelerate and possibly arrest (($dK/d(a/W) < 0$).

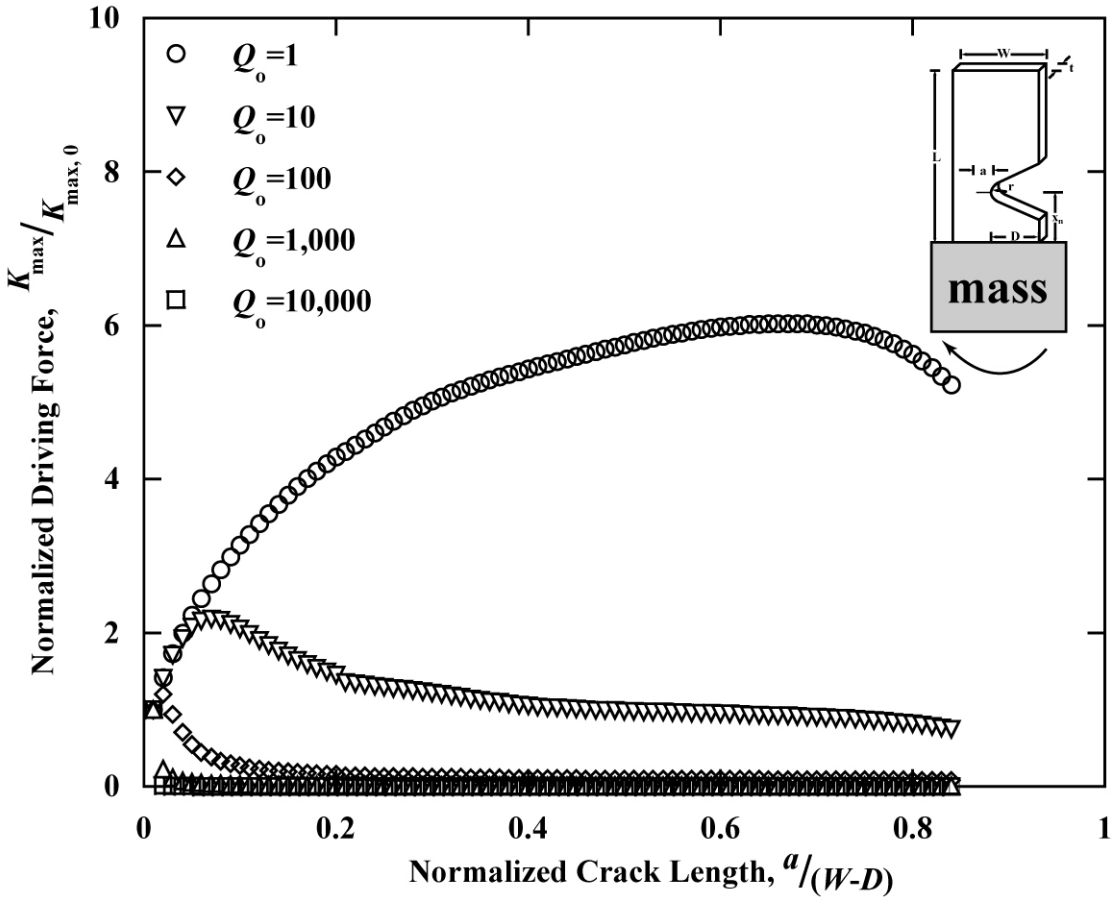

Figure 9. Stability of a fatigue crack in the resonant-loaded fatigue characterization structure (Figure 1) predicted by the lumped dynamic model. The normalized driving force for crack advance, $K_{max}/K_{max,0}$, is shown as a function of normalized crack length, $a/(W - D)$, for the notched cantilever-beam specimen within this structure. The behavior of this characterization structure is similar to that of systems modeled using existing fracture-mechanics solutions. In heavily damped systems (i.e., low Q_0), the fatigue crack will accelerate ($dK/d(a/W) > 0$). As the damping in the system is decreased (i.e., increasing Q_0), the crack will decelerate and possibly arrest (($dK/d(a/W) < 0$).

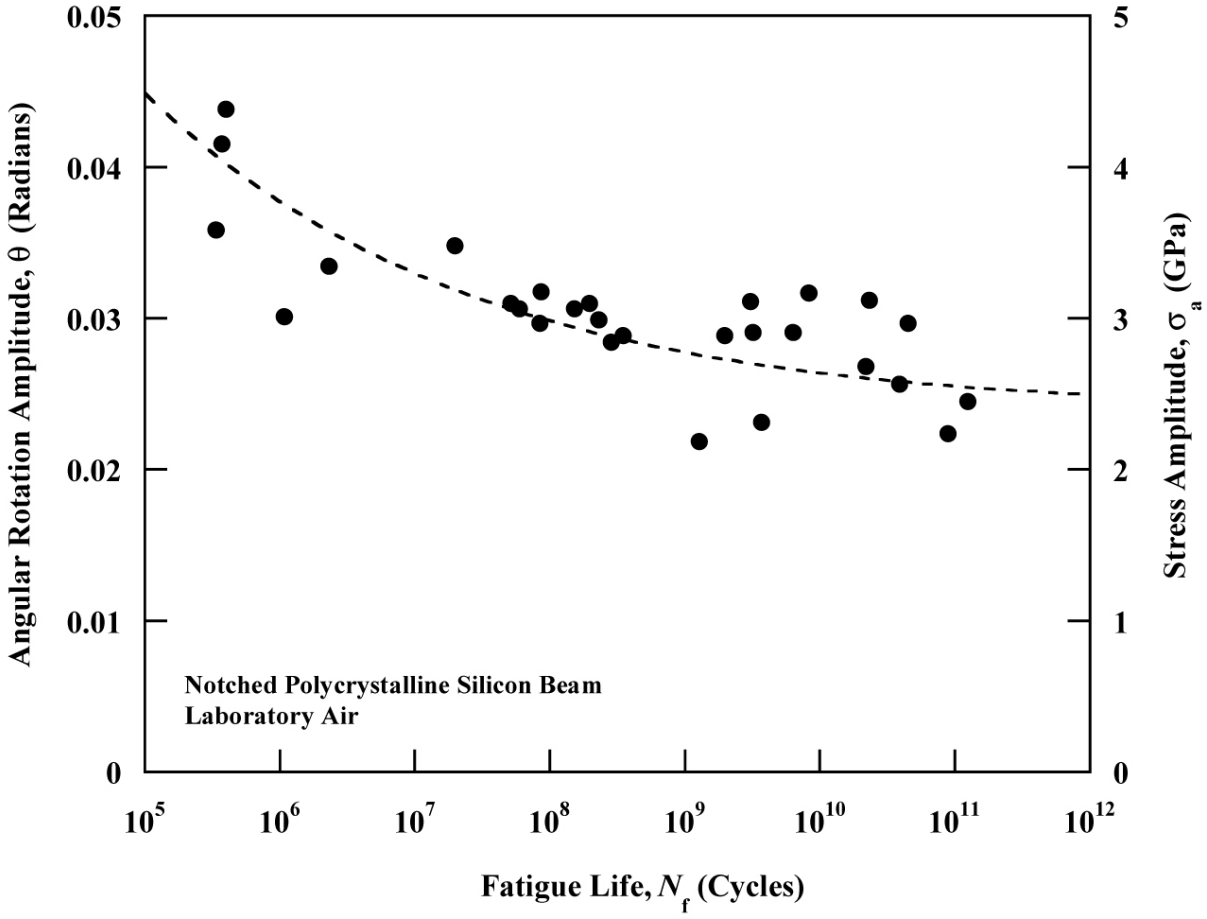

Figure 10. Typical stress-life (*S*/*N*) fatigue behavior of ~2 μm-thick, polycrystalline silicon obtained using the micron-scale fatigue characterization structure under fully reversed, tension-compression loading at 40 kHz in moist room air (Muhlstein, et al., 2000; Muhlstein, et al., 2001a).

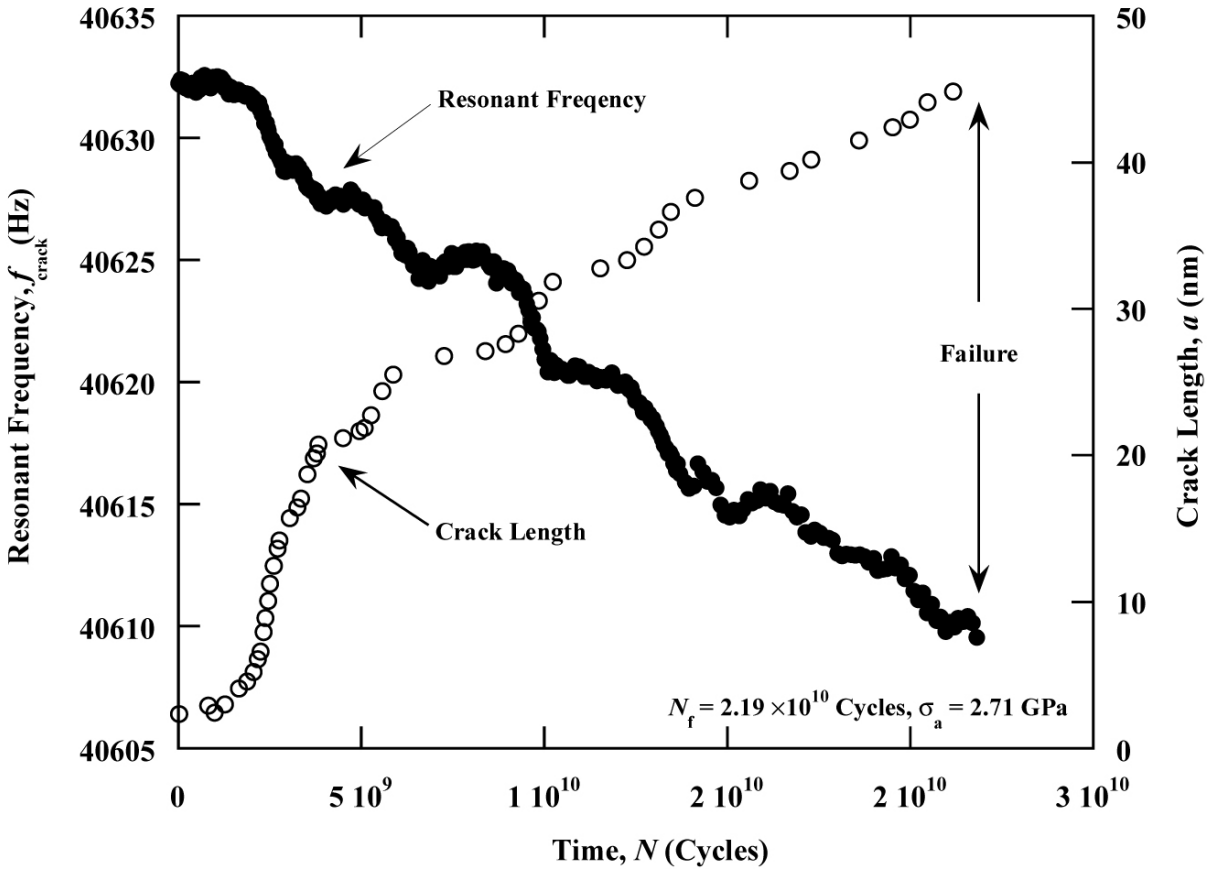

Figure 11. Damage accumulation in polycrystalline silicon, shown by experimentally measured decrease in resonant frequency, f_{crack}, with time during the fatigue test ($N_f = 2.19 \times 10^{10}$ cycles at $\sigma_a = 2.71$ GPa), with the corresponding computed increase in crack length a.

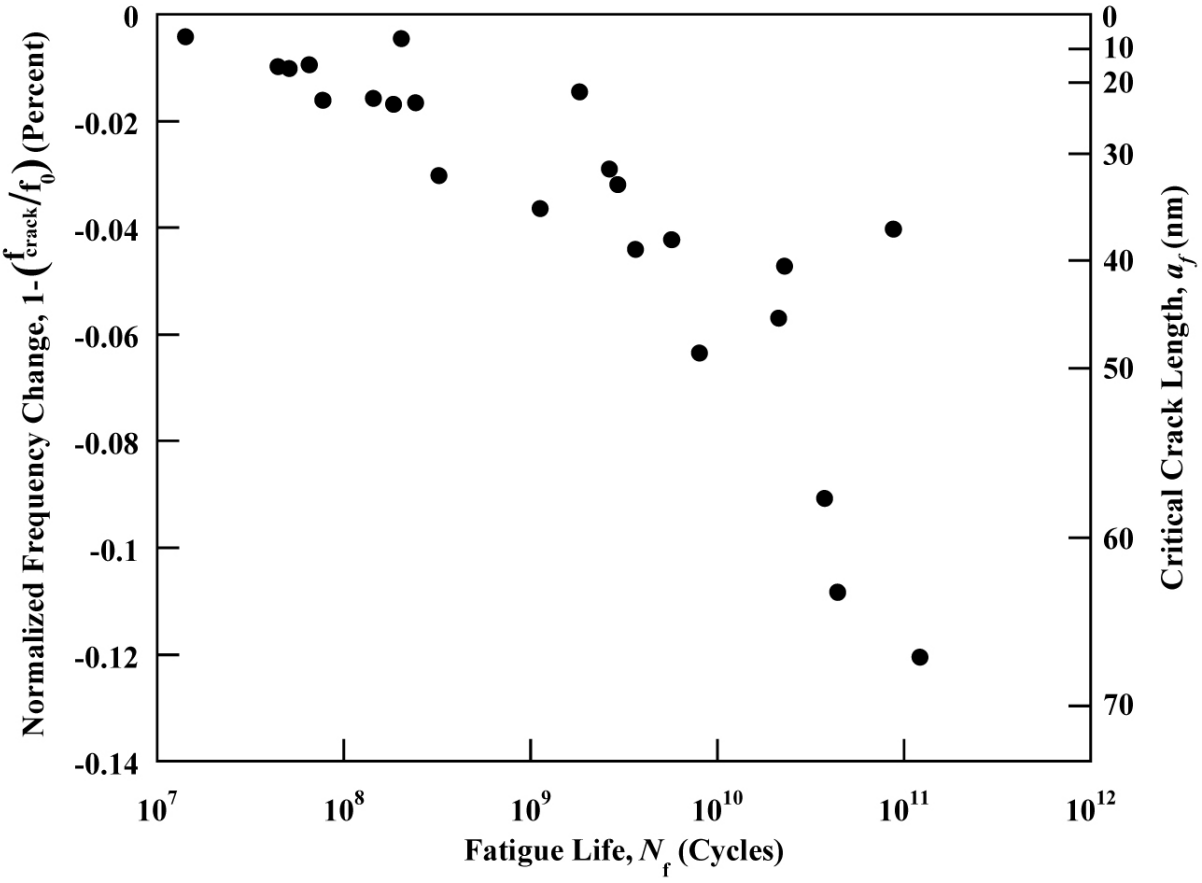

Figure 12. Decrease in normalized natural frequency, 1- (f_{crack}/f_0), and the associated final crack size, a_f, as a function of specimen life.

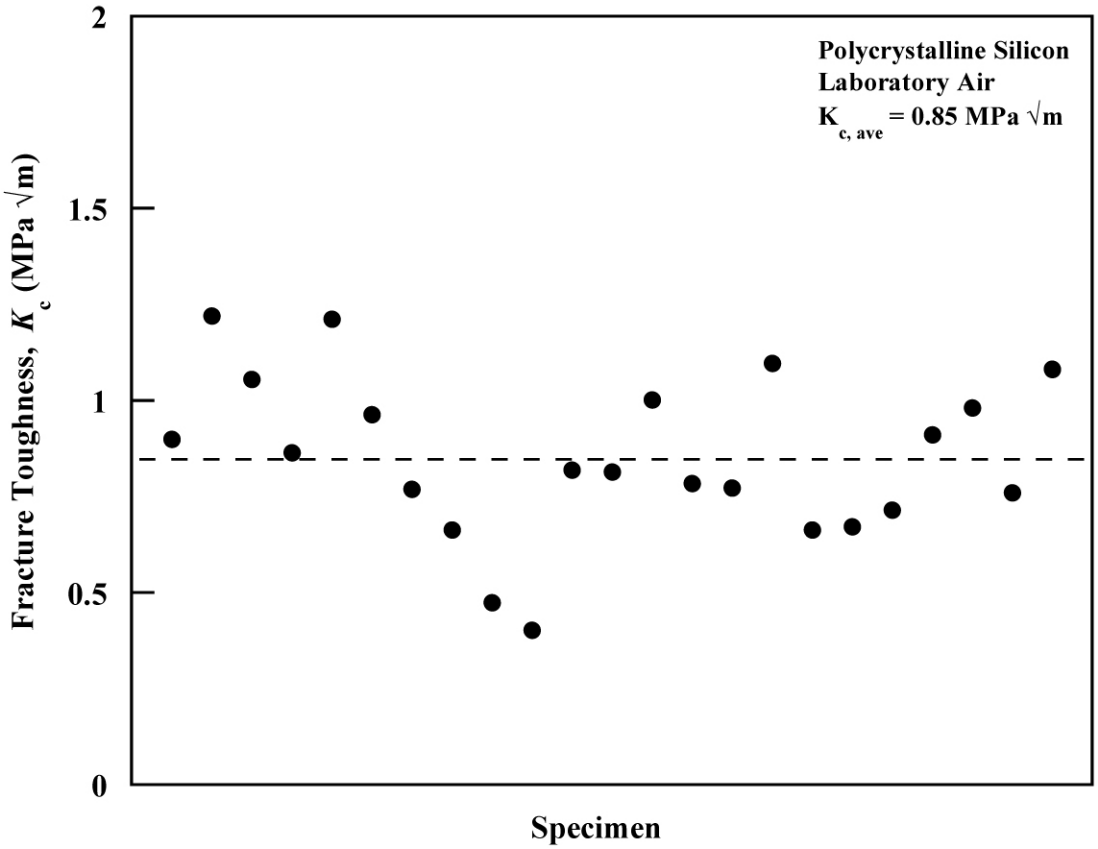

Figure 13. Computed fracture toughness, K_c, values determined from the estimated crack length immediately prior to failure, i.e., the critical crack size, a_c, for the given applied stress amplitude. The average fracture toughness (dashed line) was calculated to be 0.85 MPa√m.

Table 1. Fracture-mechanics solutions for the mode I stress-intensity factor, K_I, and compliance, s, of the edge-cracked beam in bending, edge-cracked plate in tension, and the center-cracked plate in tension geometries (Tada, et al., 2000).

Description	$K_I = \sigma\sqrt{\pi a}\cdot f\left(\frac{a}{W}\right)$	$s = \frac{1}{k}$
Center-Cracked Sheet in Tension	$f\left(\frac{a}{W}\right) = \left\{1 - 0.025\left(\frac{a}{W}\right)^2 + 0.06\left(\frac{a}{W}\right)^4\right\}\sqrt{\sec\left(\frac{\pi a}{2W}\right)}$	$s\left(\frac{a}{W}\right) = \frac{2a}{EWt}\left(-1.071 + 0.25\left(\frac{a}{W}\right) - 0.357\left(\frac{a}{W}\right)^2 + 0.121\left(\frac{a}{W}\right)^3 - 0.047\left(\frac{a}{W}\right)^4 + 0.008\left(\frac{a}{W}\right)^5 - 1.071\cdot\frac{\log\left(1-\frac{a}{W}\right)}{\frac{a}{W}}\right) + \frac{L}{2EWt}$
Edge-Cracked Sheet in Bending	$f\left(\frac{a}{W}\right) = \frac{6\sqrt{2\tan\left(\frac{\pi a}{2W}\right)}}{\cos\left(\frac{\pi a}{2W}\right)}\left[0.923 + 0.199\left\{1 - \sin\left(\frac{\pi a}{2W}\right)\right\}^4\right]$	$s_\theta\left(\frac{a}{W}\right) = \frac{24}{EW^2}\left(\frac{a/W}{1-a/W}\right)^2\left\{5.93 - 19.69\left(\frac{a}{W}\right) + 37.14\left(\frac{a}{W}\right)^2 - 35.84\left(\frac{a}{W}\right)^3 + 13.12\left(\frac{a}{W}\right)^4\right\} + \frac{12L}{EW^3t}$
Single-Edge Notched Sheet in Tension	$f\left(\frac{a}{W}\right) = \sqrt{\frac{2W}{\pi a}\tan\left(\frac{\pi a}{2W}\right)}\cdot\frac{0.752 + 2.02\left(\frac{a}{W}\right) + 0.37\left(1 - \sin\left(\frac{\pi a}{2W}\right)\right)^3}{\cos\left(\frac{\pi a}{2W}\right)}$	$s\left(\frac{a}{W}\right) = \frac{2a}{EWt}\left(\frac{a/W}{(1-a/W)^2}\right)\left\{0.99 - \frac{a}{W}\left(1-\frac{a}{W}\right)\left(1.3 - 1.2\left(\frac{a}{W}\right) + 0.7\left(\frac{a}{W}\right)^2\right)\right\} + \frac{L}{2EWt}$

Table 2. Curve fits of the modal and fracture-mechanics solutions for the notched, cantilever beam in the fatigue characterization structure shown in Figure 1.

Description	**Validity**	**Function**
Natural Frequency	$0 < \frac{a}{(W-D)} \le 0.85$	$\frac{f_{crack}}{f_0} = 1.004 - 0.07804\left(\frac{a}{(W-D)}\right) - 8.6569\left(\frac{a}{(W-D)}\right)^2 + 51.736\left(\frac{a}{(W-D)}\right)^3 - 201.93\left(\frac{a}{(W-D)}\right)^4 + 508.61\left(\frac{a}{(W-D)}\right)^5 - 815.53\left(\frac{a}{(W-D)}\right)^6 + 801.57\left(\frac{a}{(W-D)}\right)^7 - 439.42\left(\frac{a}{(W-D)}\right)^8 + 102.78\left(\frac{a}{(W-D)}\right)^9$
Nondimensional Compliance	$0 < \frac{a}{(W-D)} \le 0.2$	$sEt = 3.9856\times10^{11} + 2.441\times10^{9}\left(\frac{a}{(W-D)}\right) + 1.0302\times10^{13}\left(\frac{a}{(W-D)}\right)^2 - 1.021\times10^{14}\left(\frac{a}{(W-D)}\right)^3 + 9.5484\times10^{14}\left(\frac{a}{(W-D)}\right)^4 - 6.5976\times10^{15}\left(\frac{a}{(W-D)}\right)^5 + 3.1801\times10^{16}\left(\frac{a}{(W-D)}\right)^6 - 9.8133\times10^{16}\left(\frac{a}{(W-D)}\right)^7 + 1.7071\times10^{17}\left(\frac{a}{(W-D)}\right)^8 - 1.2397\times10^{17}\left(\frac{a}{(W-D)}\right)^9$
Nondimensional Compliance	$0.2 < \frac{a}{(W-D)} \le 0.85$	$sEt = 3.5995\times10^{11} + 4.421\times10^{12}\left(\frac{a}{(W-D)}\right) - 1.2201\times10^{14}\left(\frac{a}{(W-D)}\right)^2 + 1.5956\times10^{15}\left(\frac{a}{(W-D)}\right)^3 - 1.0488\times10^{16}\left(\frac{a}{(W-D)}\right)^4 + 3.9005\times10^{16}\left(\frac{a}{(W-D)}\right)^5 - 8.5419\times10^{16}\left(\frac{a}{(W-D)}\right)^6 + 1.0923\times10^{17}\left(\frac{a}{(W-D)}\right)^7 - 7.5486\times10^{16}\left(\frac{a}{(W-D)}\right)^8 + 2.182\times10^{16}\left(\frac{a}{(W-D)}\right)^9$
Stress Intensity Factor Geometric Function	$0 < \frac{a}{(W-D)} \le 0.85$	$f\left(\frac{a}{(W-D)}\right) = 1.7672 - 12.179\left(\frac{a}{(W-D)}\right) + 86.447\left(\frac{a}{(W-D)}\right)^2 - 310.86\left(\frac{a}{(W-D)}\right)^3 + 291.74\left(\frac{a}{(W-D)}\right)^4 + 1890.8\left(\frac{a}{(W-D)}\right)^5 - 7699.9\left(\frac{a}{(W-D)}\right)^6 + 12676\left(\frac{a}{(W-D)}\right)^7 - 10091\left(\frac{a}{(W-D)}\right)^8 + 3203\left(\frac{a}{(W-D)}\right)^9$